Numerical simulation study in a three-dimensional backward-facing step flow.

Rogério Gonçalves dos Santos, roger7@fem.unicamp.br
José Ricardo Figueiredo, jrfigue@fem.unicamp.br
University State of Campinas - UNICAMP Mechanical Engineering Faculty - Energy Department, PO Box: 6122 - Zip Code: 13083-970 - Campinas - SP - Brazil

Abstract.*The classic backward-facing incompressible step flow was studied. The importance of the three-dimensional numerical simulation for this case was highlighted by comparison with two-dimensional results. Locations of detachment and reattachment, as well as velocity profiles, were obtained as functions of Reynolds number. The Unified Finite Approach Exponential-type Scheme (UNIFAES) was employed in the discretization of the advective and viscous fluxes of the Navier-Stokes equations in primitive variables. Semi-staggered mesh was used. The momentum equations are integrated explicitly after the solution of a Poisson pressure that enforces mass conservation. Richardson extrapolation is employed to estimate the correct solutions. As should be expected, three-dimensional simulation provided better agreement with experiments than two-dimensional.*

Keywords: *backward-facing step flow, Numerical Simulation, UNIFAES*

1. INTRODUCTION

Backward-facing step flows represents a kind of problem with enormous importance in industrial applications. The detachment and reattachment points in the flow and its structure determine, for example, the local heat and mass transfer in a gas turbine. Understandably, the classic backward-facing incompressible step flow has been used extensively to test numerical methods. The importance of this test case motivated experimental investigation in laboratory models as the works of Armaly *et al.* (1983) and Lee and Mateescu (1998), which was chosen here for comparison purposes.

The two dimensional solutions tend to closely approach the numerical results until Reynolds numbers about 700. For higher values, the distance between experiments and numerics tend to increase, which has been attributed to the three dimensionality of the actual flow. The aim of the present work is to check this hypothesis.

2. METHODOLOGY

The Unified Finite Approach Exponential-type Scheme (UNIFAES) was employed in the discretization of the advective and viscous fluxes of the Navier-Stokes equations in primitive variables with the semi-staggered mesh. The momentum equations are integrated explicitly after the solution of a Poisson pressure that enforces mass conservation. Richardson extrapolation is employed to estimate the correct solutions.

2.1 Mesh

The present simulation uses the semi-staggered mesh structure, which combines vertex collocated velocity components and cell-centered pressure, as indicated in Fig. 1.

This mesh, much less used then either the staggered mesh or the cell-center collocated mesh, was presented first by Kuznetsov (1968). It was applied by Fortin and Teman (1971) and by Ladevèze and Peyret (1974) using the projection method which, according to Peyret and Taylor (1983), seems to be more efficient in the MAC mesh, what may explain its rare use.

However, a systematic comparison between the semi-staggered, staggered, cell-center collocated and vertex collocated meshes in the lid driven hydrodynamic cavity test problem, with explicit time integration, Figueiredo and Oliveira (2009a,b) indicated that the stability and the accuracy of the semi-staggered mesh is comparable to the staggered and the cell-center collocated meshes.

Analogously to the collocated meshes, the collocated velocity components of the semi-staggered mesh simplify the computation of the momentum fluxes, since the influence coefficients are the same for both momentum components. On the other side, the semi-staggered mesh shares with the staggered mesh the simple closure of the pressure equations, by maintaining the boundary velocities when taking the numerical divergence of the local momentum equation. Also, the semi-staggered mesh, as well as the vertex collocated mesh, allows the use of entirely regular spacing of both velocity components.

As both collocated meshes, the semi-staggered mesh produces oscillating pressure fields. A momentum interpolation procedure analogous to the Rhie and Chow is possible, that smoothes the pressure field at the price of loosing the strict observance to the numerical continuity equation. Alternatively, such procedure can also be used only as post processing,

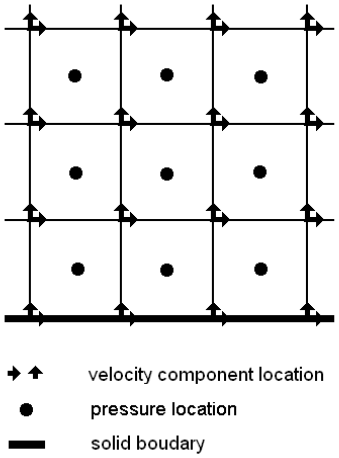

Figure 1. Semi-staggered mesh

without perturbing the solenoidal velocity field, in order to smooth the pressure field.

2.2 UNIFAES

The present work employs the Unified Finite Approach Exponential-type Scheme, UNIFAES, to compute the advective and viscous terms of the momentum equations. This scheme belongs to a class of schemes whose interpolating functions are obtained as exact solutions of a one dimensional linear equation, which somehow approximates the equation of interest. Let us consider the three-dimensional momentum transport equation in non-dimensional form, in terms of a dummy variable ϕ :

$$\frac{\partial \phi}{\partial t} + Re\frac{\partial (u\phi)}{\partial x} + Re\frac{\partial (v\phi)}{\partial y} + Re\frac{\partial (w\phi)}{\partial z} - \frac{\partial^2 \phi}{\partial x^2} - \frac{\partial^2 \phi}{\partial y^2} - \frac{\partial^2 \phi}{\partial z^2} = S \tag{1}$$

The exponential-type schemes use as interpolating curve the exact solution of the one-dimensional equation:

$$Reu\frac{d\phi}{dx} - \frac{d^2\phi}{dx^2} = K \tag{2}$$

This linear equation approximates the transport Eq.(1) around each boundary cell, by assuming the velocity to be locally constant, as well as the cross advective and diffusive fluxes, transient and source terms of the partial Eq.(1), which are represented by the non-homogeneous term. Such schemes could be expressively called Locally Analytic for their conception. Indeed such name was adopted by one particular scheme of the class (LOADS). Alternatively they may be called Exponential-type Schemes, since the exponential function appears in their interpolating curves and in their influence coefficients.

The class of Exponential-type schemes founded upon one-dimensional generating equations started with the Allen and Southwells finite differencing exponential scheme (Allen and Southwell, 1955). The methodology due to Allen was rediscovered by other authors using finite differencing, finite element and, particularly, finite volume methods. A brief review of such work is presented by Figueiredo and Oliveira (2009b), the present paper concentrates on the finite volume schemes.

The first exponential schemes proposed in the finite volume approach (Spalding, 1972; Raithby and Torrance, 1970) were based on a homogeneous generating equation associated to Eq.2, so loosing much of the similarity with the original equation. At the price of greater algorithmic complexity and bigger computational time spending, the non-homogeneous generating equation was recovered by the finite volume schemes Locally Analytic Differencing Scheme, LOADS, (Wong and Raithby, 1979), Flux-Spline Scheme, (Varejão, 1979; Karki *et al.*, 1989) and, at last, the Unified Finite Approaches Exponential-type Scheme, UNIFAES (Figueiredo, 1997).

All those schemes are naturally upwinded (Calhoon Jr. and Roach, 1997), in the sense that the influence coefficients of the upwind neighbor nodes become increasingly dominant as the cell Reynolds number increases, although the computational molecule remains symmetric except at the limit for infinite Reynolds numbers.

All exponential-type schemes are asymptotically second order, but at high Reynolds numbers the Allen and Southwell scheme and the simple Exponential Scheme approach the first order upwind scheme, justifying some criticisms to their slow spatial convergence (Leonard and Drummond, 1975). However, the exponential-type finite volume schemes based

on non-homogeneous generating equations, namely LOADS, Flux-Spline and UNIFAES, are effectively second order at any Reynolds number, being not liable to Leonard and Drummond's criticism.

The greater computational time spending of the exponential function compared to polynomial discretizations is another source of criticism which, on one hand, motivated the development of approximations such as the Power-Law Scheme (Patankar, 1980) and Padé approximants (Axelsson and Gustafsson, 1979). The Power-Law approximation was also employed in UNIFAES (Figueiredo and Llagostera, 1999; Llagostera and Figueiredo, 2000b,a).

UNIFAES was initially submitted to a series of tests representing eigenfunctions of the linear advective-diffusive transport equation on a uniform flow field (Figueiredo, 1997). It showed stability even at Peclet numbers as high as 109 and very good accuracy in all eigenfunctions, generally overcoming the central differencing, the simple exponential and LOADS. It presented no significant effects of the flow-to-grid angle. The distance of UNIFAES to the other schemes increased for crescent Peclet numbers. On the other side, all schemes tended to produce equally higher errors as the function eigenvalue increased.

Then UNIFAES was submitted to the Smith and Hutton test problem, concerning the transport of a scalar in a prescribed curved velocity field, for Peclet numbers up to 106 (Figueiredo and Llagostera, 1999). Again it presented very good performance, generally overcoming the other schemes, except the central differencing in a range of Peclet numbers where this scheme showed extremely high accuracy and unusual stability up to Peclet number 10,000. It also presented very good performance in simple one-dimensional tests concerning grid irregularity (Llagostera and Figueiredo, 2000b,a).

Then, the Power-Law form of UNIFAES was applied to the thermal transport equation on a buoyant Darcian porous flows involving natural and mixed convection in different geometries (Figueiredo and Llagostera, 1999; Llagostera and Figueiredo, 2000b,a). Some comparisons with the simple Power Law scheme also showed the crescent superiority of UNIFAES as the Rayleigh number increased.

Finally, the comparison of UNIFAES with central differencing and the simple exponential scheme was extended to the case of the incompressible Navier-Stokes equations in primitive variables, considering all fundamental mesh structures, employing the classic test problems of the 2D lid-driven cavity flow in the standard form (with uniform lid velocity) and in the regularized form (that removes the singularity at the lid corners) (Figueiredo and Oliveira, 2009b,a). The reader is also referred to such papers for details on the governing equations, on the method of solution and on the methodology of Richardson extrapolation.

A simplified presentation of the Finite Volume Exponential-type Schemes for discretization of the advective and viscous transport of momentum, particularly UNIFAES, is given here. Algebraic details are found in (Figueiredo, 1997; Figueiredo and Llagostera, 1999).

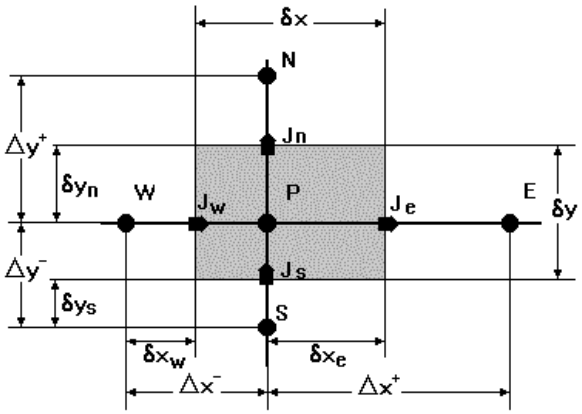

Figure 2. Rectangular control volume with the compass notation

Figure 2 reproduces a 2D rectangular control volume with the usual Finite Volume compass notation, showing the advective-viscous fluxes located at the intersection of its parallel coordinate and its orthogonal cell face. The combined net advective and viscous flux

$$A_\phi = Re\frac{\partial(u\phi)}{\partial x} + Re\frac{\partial(v\phi)}{\partial y} + Re\frac{\partial(w\phi)}{\partial z} - \frac{\partial^2\phi}{\partial x^2} - \frac{\partial^2\phi}{\partial y^2} - \frac{\partial^2\phi}{\partial z^2} \tag{3}$$

is integrated on the cell volume v and is transformed, through to the divergence theorem, into the integral of the advective-viscous flux through the cell surface. For all control volume locally analytic schemes, the integrated net flux is given by:

$$\int_v \int A_\phi dv \cong a_E(\phi_E - \phi_P) + a_W(\phi_W - \phi_P) + a_N(\phi_N - \phi_P) + a_S(\phi_S - \phi_P) + a_F(\phi_F - \phi_P) + a_B(\phi_S - \phi_B) - \psi \tag{4}$$

where

$$a_{E/W} = \pi(\pm p_{e/w})\delta y\ \delta z/\delta x^{\pm} \tag{5}$$

$$a_{N/S} = \pi(\pm p_{n/s})\delta x\ \delta z/\delta y^{\pm} \tag{6}$$

$$a_{F/B} = \pi(\pm p_{f/b})\delta x\ \delta y/\delta z^{\pm} \tag{7}$$

$$p_{e/w} = Re\ u_{e/w}\ \Delta x^{\pm} \tag{8}$$

$$p_{n/s} = Re\ v_{n/s}\ \Delta y^{\pm} \tag{9}$$

$$p_{f/b} = Re\ v_{f/b}\ \Delta z^{\pm} \tag{10}$$

$$\pi(p) = \frac{p}{exp(p) - 1} \tag{11}$$

$$\psi = [K_e\Delta x^{+}\chi(p_e) - K_w\Delta x^{-}\chi(p_w)]\delta y + [K_n\Delta y^{+}\chi(p_n) - K_s\Delta y^{-}\chi(p_s)]\delta x + [K_f\Delta z^{+}\chi(p_f) - K_b\Delta z^{-}\chi(p_b)]\delta z \tag{12}$$

$$\chi(p) = \frac{\pi(p) - 1}{p} + R \tag{13}$$

$$R = \frac{\delta x_{e/w}}{\Delta x^{\pm}}\ \ or\ \ R = \frac{\delta y_{n/s}}{\Delta y^{\pm}}\ \ or\ \ R = \frac{\delta z_{f/b}}{\Delta z^{\pm}} \tag{14}$$

In Eqs.(5) to (10) and (14), indexes e, n and f correspond to sign +, and indexes w, s and b to sign -.

The simple exponential scheme (Spalding, 1972; Raithby and Torrance, 1970; Patankar, 1980) is recovered by assuming null K., so dismissing Eqs. (12) to (14). The complete equations are relevant for LOADS and UNIFAES, and, with minor changes, for the Flux-Spline scheme.

In UNIFAES, the information about K is provided by the finite differencing approach that led to the Allen and Southwell scheme (Allen and Southwell, 1955). The Allen and Southwell exponential scheme computed the analogue of the net advective and diffusive fluxes in non conservative form by employing the generating equation analogous to Eq. 2, but centered on node P. Generalizing the Allen and Southwell scheme for irregularly spaced grids one obtains:

$$K_p = (\phi_p - \phi_E)\Pi^{+} + (\phi_P - \phi_W)\Pi^{-} \tag{15}$$

where $\Pi^{\pm}$ was put by Llagostera and Figueiredo (2000a,b) in a form adequate for using any approximation of the function :

$$\Pi^{\pm} = \frac{Re\ u_p\ \pi(\pm p_u^{\pm})}{\Delta x^{\pm}[\pi(-p_u^{-}) - \pi(p_u^{+})]} \tag{16}$$

where

$$p_u^{\pm} = Re\ u_p\ \Delta x^{\pm} \tag{17}$$

In uniform grids, Eq. (16) reduces to the original Allen and Southwell scheme:

$$\Pi^{\pm} = \frac{\pi(\pm p_u^{\pm})}{\Delta x^2} \tag{18}$$

In UNIFAES, the source term $K_e^{i,j,k}$, for instance, is found by linear interpolation of the generalized Allen and Southwell estimates of K_p on the nodes (i, j, k) and $(i+1, j, k)$. Although the Allen and Southwell scheme is non-conservative, its use in UNIFAES maintains numerical conservation because $K_e^{i,j,k} = K_w^{i+1,j,k}$, so that $J_e^{i,j,k} = J_w^{i+1,j,k}$. The 3D computational molecule around node (i, j, k) involves the immediate neighbors $(i \pm 1, j, k)$, $(i, j \pm 1, k)$ and $(i, j, k \pm 1)$ and also the remote nodes $(i \pm 2, j, k)$, $(i, j \pm 2, k)$ and $(i, j, k \pm 2)$. At the cell boundaries neighbor to the domain frontiers, is linearly extrapolated from the closest internal nodes, dismissing the remote node outside the domain.

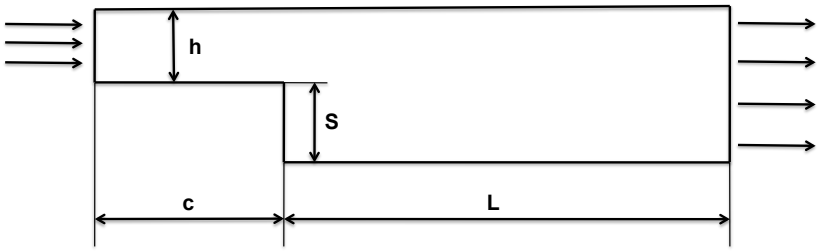

Figure 3. Sketch of the step geometry defining various geometrical parameters.

2.3 Numerical setup

The domain of study was the same of Lee and Mateescu (1998). The expansion ratio ER=(S+h)/h tested was 2.0. The characteristic dimension D is the neck hydraulic diameter, $D = 2h$. The definition of Reynolds is the same of Armaly *et al.* (1983) and is calculated as:

$$Re = \frac{VD}{\nu} \tag{19}$$

where V is the mean velocity at the entrance and ν is the kinetic viscosity.

The dimensionless values used were h=0.5, S=0.5, L=20 for 100≤Re≤600, L=30 for Re≥800, width W=20 and the entrance channel c=5.0.

A parabolic profile representative of a fully developed entrance chanel flow was imposed in the inlet region, therefore, the mean velocity at the inlet is $2/3$ of the maximum inlet velocity. The walls are hipermeable and non-slip. Homogeneous Neumann boundary condition were assumed for the velocity components at the domain outlet.

Two different sets of mesh sizes Δx, Δy and Δz were simulated for each Reynolds number. For 100≤Re≤600, the less refined one had Δx=0.25, Δy=0.025 and Δz=0.5, in the most refined case Δx=0.1666, Δy=0.01666 and Δz=0.333. For 700≤Re≤900, the less refined one had Δx=0.15625, Δy=0.015625 and Δz=0.625, in the most refined case Δx=0.125, Δy=0.0125 and Δz=0.5. The pair of numerical results for each case was used to estimate the numerical error by mean of Richardson extrapolation.

Schematic location of the two recirculation zones that can be present in the flow and the three main points of detachment or reattachment can be seen at Fig. 4.

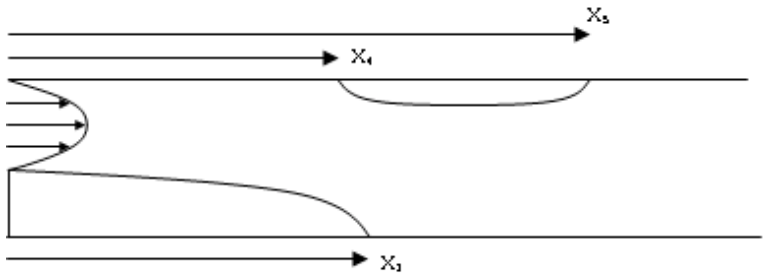

Figure 4. Location of detachment and reattachment points

3. RESULTS

Figure 5 shows the profiles of the u velocity at $z = 10.0$ for three different x, $x = 8.5$, $x = 12.5$ and $x = 20.0$ in function of entrance channel length for Re=600, remembering that the expansion step is located at $x = 5.0$. By this figure it is possible to analyze the evolution of "u" velocity profile. At $x = 8.5$ we have only the first recirculation zone accting in the bottom of the channel, at $x = 12.5$ this recirculation zone at bottom no more acte and the second one at the top can be seen, this one has a small intensity when compared with the first one. And finally at $x = 20.0$ the flow takes an aspect parabolic, with means the we are far enough form the step region and the flow begin to be developed.

Figure 7 shows the profiles of the u velocity at $x = 10.0$ for three different z, $z = 1.25$, $z = 2.5$ and $z = 10.0$ for Re=700. As the with is 20.0, $z = 1.25$ is located near the lateral wall, $z = 10.0$ is located in the middle of the channel and $z = 2.5$ between the two. At $x = 10.0$ for Re=700, we are at a zone where coexist the bottom and top recirculation zone. The main purpose of this figure is to show the 3D characteristic of this flow, acutely in this region where we have the two recirculation zone acting this characteristic is more pronounced. In the figure its possible to see comparing the

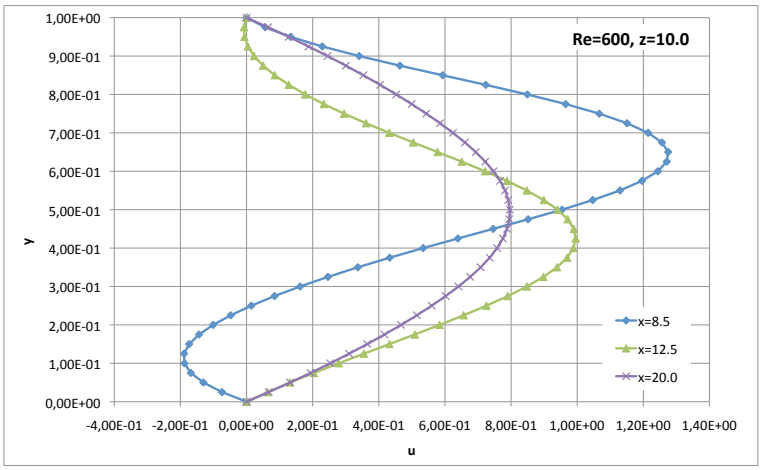

Figure 5. Re=600, Profiles of u velocity at $z = 10.0$ for $x = 8.5$, $x = 12.5$ and $x = 20.0$.

curves to $z = 1.25$ and $z = 10.0$ that the y value to maximum value is different and the intensity of the recirculation is smaller near the wall ($z = 1.25$) when compared with the middle of the channel ($z = 10.0$).

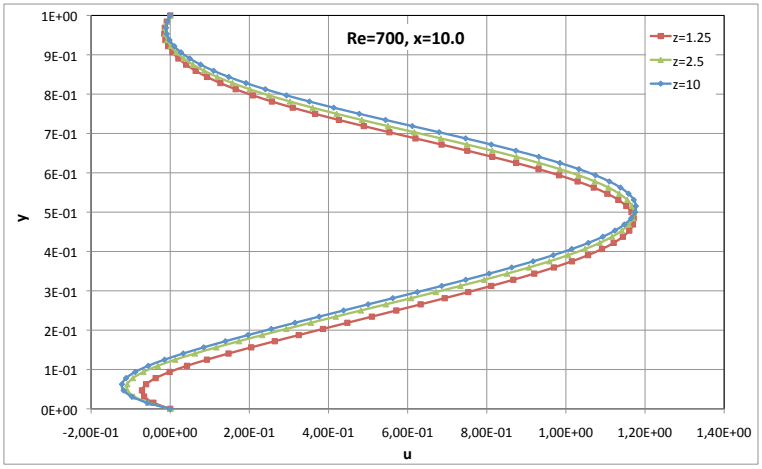

Figure 6. Re=700, Profiles of u velocity at $x = 10.0$ for $z = 1.25$, $z = 2.5$ and $z = 10.0$.

Figure 7 shows the profile of the u velocity in function of the z for three different lines, the first one at $x = 7.5$ and $y = 2.5$ inside the bottom recirculation zone, the second one at $x = 7.5$ and $y = 7.5$ just above the first bubble in the bottom wall, finally, the third one at $x = 12.5$ and $y = 7.5$ represents a region just below the recirculation zone at the top wall. Analyzing the three profiles it is possible to see the 3D characteristic of this flow appears in a special way in the region near the recirculation zones and the lateral wall, where the u velocity varies with z.

Figure 8 shows the variation of the location of the reattachment point at the lower wall x1 as function of the Reynolds numbers for three different z position ($z = 2.0$, $z = 5.0$ and $z = 10.0$). As its possible to see, the 3D characteristic of the flow start to appear for Re=300, when the influence of the lateral wall in the flow, change the position of the reattachment point for $z = 2.0$.

Variation of the location of detachment and reattachment points at the upper wall x_4 and x_5 as function of the Reynolds numbers are plotted at Fig. 9 and Fig. 10 for three different z position ($z = 2.0$, $z = 5.0$ and $z = 10.0$). Fig.9 shows a huge influence of the wall proximity in the dettachement point x_4, the upper recirculation zone starts early to $z = 2.0$ when compared with the regions in the middle of the channel. This is duo, the proximity of the 2 two recirculation zone (bottom and upper one), as said before, what reinforce the 3D characteristic of the flow in this zone. However, at fig.10 its possible to see that the region where the upper recirculation zone finished is practically independent of z, as the influence of the bottom recirculation zone is almost null.

Figure 11 shows the variation of the location of the reattachment point at the lower wall x_1 as function of the Reynolds numbers in the middle of the channel, comparing the present 3D data with a 2D simulation using a analogous methodology of this work (Santos *et al.*, 2010) and the original experimental data from Lee and Mateescu (1998).

The 2D and 3D simulations x_1 values obtained for the middle of the channel are very similar. This is duo, the small influence of the 3D characteristc of the flow in middle of the channel and the Reynolds number simulated that not represent the turbulence flow (Lee and Mateescu (1998) says that the transitional flow regime start at Re=1150).

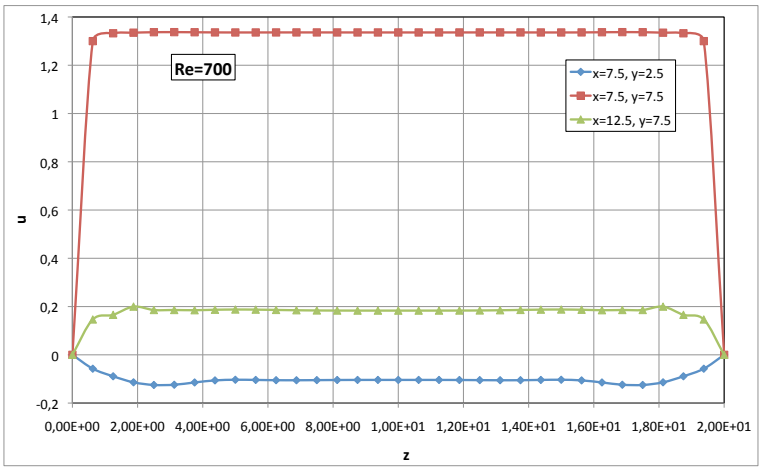

Figure 7. Re=700, Profiles of u velocity at three different lines, $x = 7.5$ and $y = 2.5$, $x = 7.5$ and $y = 7.5$, $x = 12.5$ and $y = 7.5$

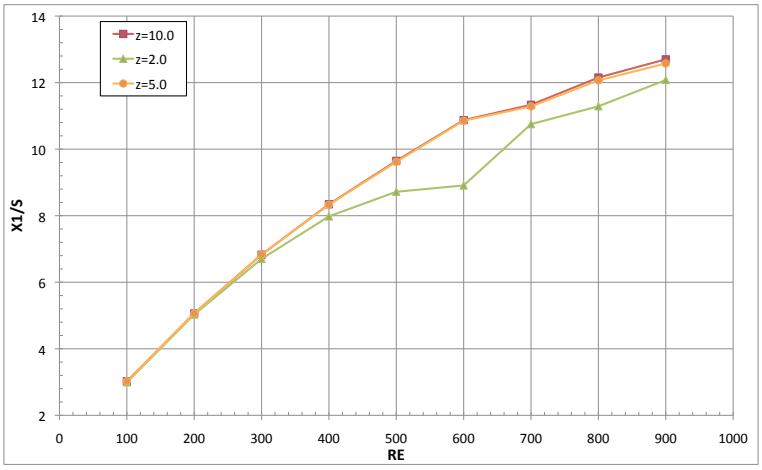

Figure 8. Variation of location of reattachment points at lower wall x_1 with Reynolds numbers for $z = 2.0$, $z = 5.0$ and $z = 10.0$.

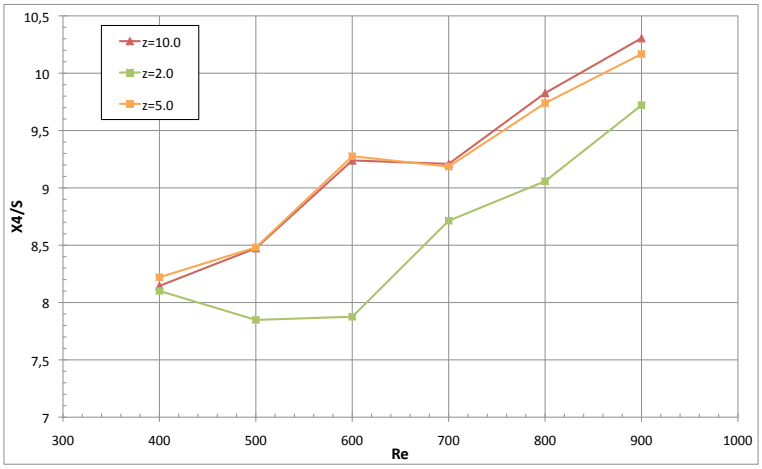

Figure 9. Variation of location of reattachment points at upper wall x_4 with Reynolds numbers for $z = 2.0$, $z = 5.0$ and $z = 10.0$.

Numerical simulation has a good agreement with the experimental data until Re=700, when both numerical simulation results start to have bigger differences with the experimental results.

In order to evaluate the errors of previous calculation, Table 1, exposes the buble sizes obtained with both refinement levels, together with the corresponding Richardson extrapolation considering second order convergence.

Variation of the location of detachment and reattachment points at the upper wall x_4 and x_5 as function of the Reynolds

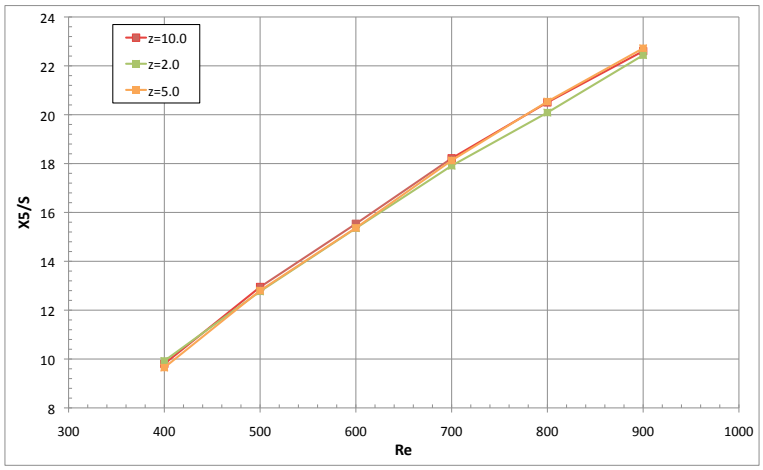

Figure 10. Variation of location of reattachment points at upper wall x_5 with Reynolds numbers for $z = 2.0$, $z = 5.0$ and $z = 10.0$.

Table 1. X_1 values for the two different meshes and the corresponding Richardson extrapolation value

Re	Mesh1	Mesh 2	Richardson Extrapolation
100	3.3863	3.2298	3.1046
200	5.4376	5.2721	5.1396
300	6.8929	6.8573	6.8289
400	8.3559	8.3492	8.3439
500	9.5146	9.5879	9.6466
600	10.4213	10.6720	10.8725
700	11.2253	11.1644	11.3337
800	11.9755	11.8759	12.1525
900	12.6993	12.5158	13.0256

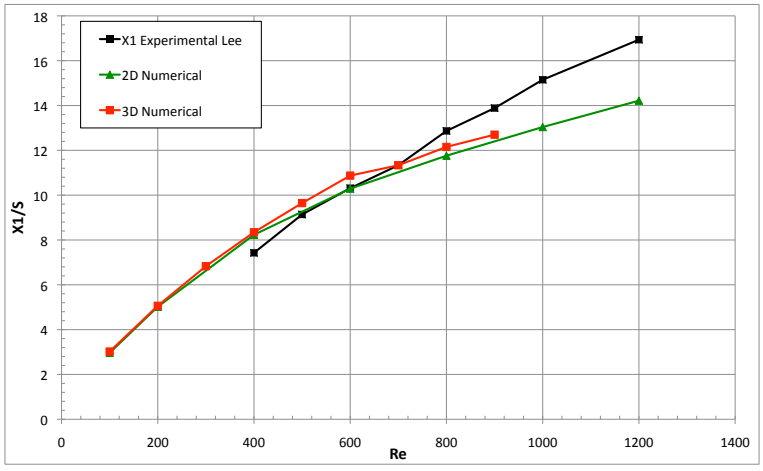

Figure 11. Variation of location of reattachment points at lower wall x_1 with Reynolds numbers. Experimental data from Lee and Mateescu (1998), presented 3D numerical data and 2D numerical data from Santos *et al.* (2010).

numbers in the middle of the channel are plotted at Fig.12 and Fig.13 . Experimental data from Lee and Mateescu (1998) are compared with the present numerical simulations and with a 2D numerical simulations from (Santos *et al.*, 2010). Experimental and numerical data have a good agreement until Re=800, when x_4 values of experimental data stabilize and x_5 increase quickly, resulting in a smaller recirculation zone when compared with the simulations.

Figure 12 (deattachement point x_4) shows for Re$\leq$600 a better agreement between 2D numerical simulations and experimental results. For Re$\geq$700 the 3D simulations is in a better agreement with the experimental data. As we can see at Fig. 13, 2D and 3D simulations have obtained very close results for x_5 location in the middle of the channel with a good agreement with experimental data for 700$\leq$Re$\leq$800.

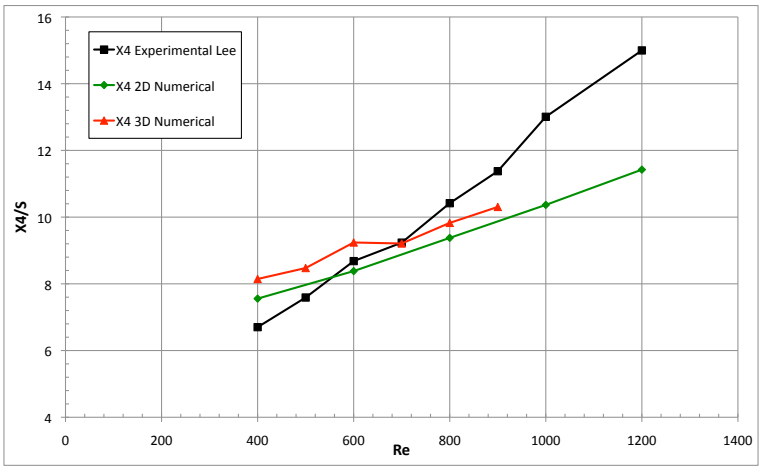

Figure 12. Variation of location of detachment point at upper wall x_4 with Reynolds numbers. Experimental data from Lee and Mateescu (1998), presented 3D numerical data and 2D numerical data from Santos *et al.* (2010).

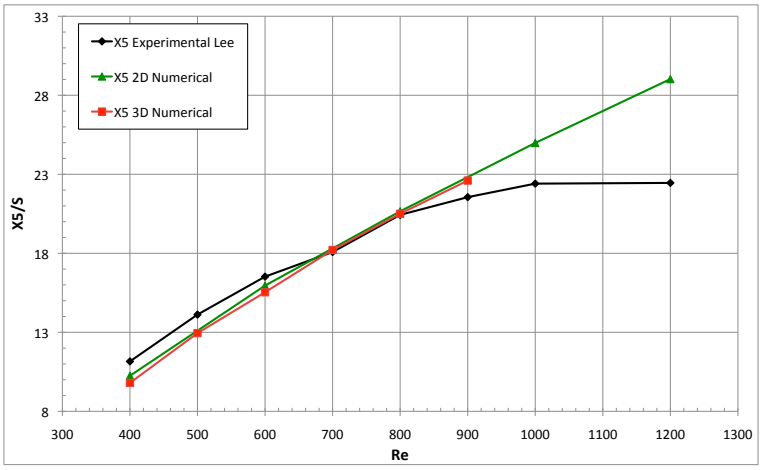

Figure 13. Variation of location of reattachment point at upper wall x_5 with Reynolds numbers. Experimental data from Lee and Mateescu (1998), presented 3D numerical data and 2D numerical data from Santos *et al.* (2010).

4. CONCLUSIONS

The influence of the 3D simulation in the numerical simulation of the classic two-dimensional backward-facing step flow was studied. Location of detachment and reattachment and velocity profile as function of Reynolds number were obtained and compared with experimental data from Lee and Mateescu (1998) and 2D numerical data from Santos *et al.* (2010).

The combination of the semi-staggered mesh with the UNIFAES discretization scheme was used in a first time in a 3D simulation and showed good stability and precision in all the cases presented here.

Results showed a small but not ignorable influence of the 3D simulation for the Reynolds number simulated in the location of the detachment and reattachment points and in the size of the recirculation zones, in a special way in the region near the lateral wall. However, the three dimensional numerical results remained practically as far from the experimental results as the two dimensional numerical results. Therefore, the most plausible explanation for the disagreement between 2D numerical solutions and experimental must be discardable. Other possibility concern the effects of perturbations in the flow, which is to be checked in a further work.

5. ACKNOWLEDGEMENTS

The authors acknowledge the financial support from research funding agencie FAPESP (Fundação de Amparo à Pesquisa do Estado de São Paulo).

6. REFERENCES

Allen, D.N.d.G. and Southwell, R., 1955. "Relaxation methods applied to determine the motion, in two dimensions, of a viscous flow past a fixed cylinder". *Quart. J. Mech. and Applied Math.*, Vol. 8, pp. 129–145.

Armaly, B., Durst, F., Pereira, J. and Schounung, B., 1983. "Experimental and theoretical investigation of backward-facing step flow". *JOURNAL OF FLUID MECHANICS*, Vol. 127, No. FEB, pp. 473–496.

Axelsson, O. and Gustafsson, I., 1979. "A modified upwind scheme for convective transport equations and the use of a conjugate gradient method for the solution of non-symmetric systems of equations". *J. Inst. Maths. Applics.*, Vol. 23, pp. 321–337.

Calhoon Jr., W.H. and Roach, R.L., 1997. "A naturally upwinded conservative procedure for the incompressible navier-stokes equations on non-staggered grids". *Computers and Fluids*, Vol. 26, No. 5, pp. 525–545.

Figueiredo, J.R., 1997. "A unified finite-volume finite-differencing exponential-type convective-diffusive fluid transport equations". *J. Braz. Society Mech. Sci.*, Vol. 3, pp. 371–391.

Figueiredo, J.R. and Llagostera, J., 1999. "Comparative study of the unified finite approaches exponential-type scheme (unifaes) and its application to natural convection in a porous cavity". *Numerical Heat Transfer, B*, Vol. 35, pp. 347–367.

Figueiredo, J.R. and Oliveira, K.P.M., 2009a. "Comparative Study of the Accuracy of the Fundamental Mesh Structures for the Numerical Solution of Incompressible Navier-Stokes Equations in the Two-Dimensional Cavity Problem". *NUMERICAL HEAT TRANSFER PART B-FUNDAMENTALS*, Vol. 55, No. 5, pp. 406–434.

Figueiredo, J.R. and Oliveira, K.P.M., 2009b. "Comparative Study of UNIFAES and other Finite-Volume Schemes for the Discretization of Advective and Viscous Fluxes in Incompressible Navier-Stokes Equations, Using Various Mesh Structures". *NUMERICAL HEAT TRANSFER PART B-FUNDAMENTALS*, Vol. 55, No. 5, pp. 379–405.

Fortin, M.; Peyret, R. and Teman, R., 1971. "Résolution numérique des equations de navier-stokes pour un fluide incompressible". *J. Mécanique*, Vol. 3, pp. 357–390.

Karki, K.C., Patankar, S.V. and Mongia, M.C., 1989. "Solution of three-dimensional flow problem using a flux-spline method". *AIAA*.

Kuznetsov, B.G., 1968. "Numerical methods for solving some problems of fluid flow". *Fluid Dynamics Transactions*, Vol. 4, pp. 85–89.

Ladevèze, J. and Peyret, R., 1974. "Calcul numérique d'une solution avec singularitè des equations de navier-stokes: Écoulement dans un canal avec variation brusque de section". *J. Mécanique*, Vol. 13, No. 3, pp. 367–396.

Lee, T. and Mateescu, D., 1998. "Experimental and numerical investigation of 2-D backward-facing step flow". *JOURNAL OF FLUIDS AND STRUCTURES*, Vol. 12, No. 6, pp. 703–716.

Leonard, B.P. and Drummond, J.E., 1975. "Why you should not use 'hybrid', 'power-law' or related exponential schemes for convective modelling - there are much better alternatives". *Int. J. Numerical Methods in Fluids*, Vol. 20, pp. 421–442.

Llagostera, J. and Figueiredo, J.R., 2000a. "Application of the unifaes discretization scheme to mixed convection in a porous layer with a cavity, using the darcy model". *J. Porous Media*, Vol. 3, No. 2, pp. 139–154.

Llagostera, J. and Figueiredo, J.R., 2000b. "Numerical study on mixed convection in a horizontal flow past a square porous cavity using unifaes scheme". *J. Braz. Soc. Mech. Sci.*, Vol. 4, pp. 583–597.

Patankar, S.V., 1980. *Numerical Heat Transfer and Fluid Flow*. McGraw-Hill.

Peyret, R. and Taylor, T.D., 1983. *Computational Methods for Fluid Flow*. Springer-Verlag.

Raithby, G.D. and Torrance, K.E., 1970. "Upstream-weighted differencing schemes and their application to elliptic problems involving fluid flow". *Computers and Fluids*, Vol. 2, pp. 191–206.

Santos, R.G., P., O.K. and R., F.J., 2010. "Influence study of the entrance channel in a two-dimensional backward-facing step flow". In *CILAMCE*.

Spalding, D.B., 1972. "A novel finite difference formulation for differential expressions involving both first and second derivatives". *Int. J. Numer. Meth. Eng.*, Vol. 4, pp. 551–559.

Varejão, L.M.C., 1979. *Flux-Spline Method for Heat and Momentum Transfer*. Ph.D. thesis, University of Minnesota.

Wong, H.H. and Raithby, G.D., 1979. "Improved finite-difference methods based on a critical evaluation of the approximation errors". *Numerical Heat Transfer*, Vol. 2, pp. 139–163.

7. Responsibility notice

The author(s) is (are) the only responsible for the printed material included in this paper